RSC Advances

PAPER

View Article Online
View Journal | View Issue

Check for updates

Cite this: *RSC Adv.*, 2026, **16**, 24852

Sulfonic-acid functionalized hypercrosslinked porous organic polymer as a highly efficient heterogeneous catalyst for synthesis of 2*H*-chromene derivatives

Siriphong Somprasong, Thanchanok Ratvijitvech, Thanakorn Tiyawarakul, Chaiwat Rujirasereesakul, Thanakorn Sitthasakul and Torsak Luanphaisarnnont *

Received 11th April 2026
Accepted 30th April 2026

DOI: 10.1039/d6ra03062a

rsc.li/rsc-advances

A sulfonic acid-functionalized hypercrosslinked porous organic polymer (HCP-H-SO_3H) with high surface area (S_{BET} = 604 m^2 g^{-1}) was successfully synthesized *via* a Friedel–Crafts alkylation of benzene and dimethoxymethane, followed by sulfonation of aromatic rings using sulfuric acid. This material was used as an efficient heterogeneous catalyst in a cyclization between various *ortho*-hydroxy aromatic aldehydes and acetylenic diesters, affording the corresponding 2*H*-chromenes in moderate to excellent yields. The material could be reused for at least five reaction cycles, suggesting the sustainable application potential of this sulfonic-acid functionalized materials as a heterogeneous acid catalyst. A mechanistic investigation using ^{13}C NMR kinetic isotope effect at natural abundance experiments provided insights into a similar nature of the rate-limiting steps in the catalytic processes of the homogeneous catalyst (*p*-toluenesulfonic acid monohydrate; PTSA·H_2O) and the heterogeneous catalyst (HCP-H-SO_3H).

1 Introduction

2*H*-Chromeme and its derivatives are prevalent heterocyclic aromatic structural units in natural products and pharmaceutical targets,[1] as well as in organic synthesis and material science.[2] Over the past several decades, numerous homogeneous catalytic methods have been disclosed for the synthesis of 2*H*-chromenes. Transition metals[3a–d] and organo-catalysts[3e–j,4] have been reported as efficient catalysts for the reaction. Recently, our research group reported a selective synthesis of 2*H*-chromenes *via* an intermolecular annulation reaction of *ortho*-hydroxy aromatic aldehydes with acetylenic diesters using a dual-organocatalytic system, a combination of *p*-toluenesulfonic acid monohydrate (PTSA·H_2O) and pyrrolidine, under mild conditions giving the products in excellent yields.[4]

Heterogeneous catalysis plays a key role in chemistry because of its eco-friendly conditions, reusability, and convenient separation from the reaction mixture.[5] Recently, functionalized hypercrosslinked porous organic polymers (HCPs) have attracted significant attention owing to their high potential applications in gas storage and separations,[6] small-molecules capture,[7] drug delivery vehicle,[8] antimicrobial materials,[9] light-harvesting and light-emitting applications,[10] sensors,[11] energy storage and conversion,[12] and catalysis of various important organic transformations.[13] There are many advantages of HCPs over other porous materials such as high surface areas, good accessibilities to a broad range of monomers, convenient surface functionalization methods, low skeleton densities, and thermal and chemical stabilities.

The use of heterogeneous catalyst for the synthesis of 2*H*-chromenes from *ortho*-hydroxy aromatic aldehydes and acetylenic diesters such as silica gel,[14] imidazole-functionalized silica nanoparticles,[15] and ZnO nanoparticles have been reported.[16] However, compared to homogeneous catalysts, these heterogeneous catalysts still have some limitations such as lower reactivity, poor selectivity of the conjugate addition products (2*H*-chromenes *versus* 4*H*-chromenes), and narrow substrate scopes.[3c–e,4] Development of a new synthetic method using a heterogeneous catalyst to overcome this limitation is therefore important. We envision that the sulfonic-acid functionalized hypercrosslinked porous organic polymer may act as a highly efficient heterogeneous catalyst for the syntheses of 2*H*-chromenes. Previous reports have used chlorosulfuric acid as a sulfonating agent for various HCPs;[17] however, the use of readily available sulfuric acid for sulfonation has not been thoroughly studied. Furthermore, although there have been reports on the use of heterogeneous acid catalysts for biomass valorization to biofuels and bioproducts[18] and various organic reactions,[19] the use of the sulfonic-acid functionalized material for mechanistically complex cyclization such as the synthesis of 2*H*-chromene derivatives has not been reported. Additionally, a mechanistic investigation to compare the reaction behaviors

---

Department of Chemistry and Center of Excellence for Innovation in Chemistry, Faculty of Science, Mahidol University, Bangkok 10400, Thailand. E-mail: torsak.lua@mahidol.ac.th

of a homogeneous sulfonic-acid catalyst and a heterogeneous sulfonic-acid catalyst has not been studied.

Herein, we reported a successful synthesis of derivatives of sulfonic-acid functionalized hypercrosslinked porous organic polymer (HCP-X-SO_3H) using readily available concentrated sulfuric acid as a sulfonating agent. We also explored the application of the material as a heterogeneous catalyst in a complex cyclization to synthesize 2*H*-chromene derivatives. In addition, we used ^{13}C NMR kinetic isotope effect experiments to study the rate-determining steps of the reaction catalyzed by homogeneous PTSA·H_2O and that catalyzed by heterogeneous HCP-H-SO_3H to compare the behaviors of the two catalysts.

2 Results and discussion

2.1 Synthesis of HCP-X-SO_3H

Preparation of the HCP-X-SO_3H involved a two-step procedure containing polymerization and sulfonation (a general reaction scheme is shown in Table 1). First, the non-functionalized hypercrosslinked porous organic polymers (HCP-X) were synthesized *via* Friedel–Crafts alkylation of benzene derivatives and dimethoxymethane using $FeCl_3$ as a mediator. The polymers were obtained as red-brown solid in excellent yield (82–>99% yield).[6f,20] For the sulfonation step, reaction optimization was performed using HCP-H as a model substrate. The reaction parameters under optimization included the concentration of H_2SO_4, the reaction temperature, and the ratio of HCP-H to H_2SO_4 (see SI). The optimized reaction conditions were conc. H_2SO_4 at 100 °C, leading to the formation of the HCP-H-SO_3H as a black solid in 78% yield. The acid concentration was determined using a back acid–base titration method (see SI). The calculated acid concentration of HCP-H-SO_3H was 4.16 mmol g^{-1}. The scope of the sulfonation was investigated using substrates with various substituents. HCP-X with sterically different substituents (X = CH_3, C_2H_5, *n*-C_3H_7, and *i*-C_3H_7) were sulfonated using the optimized reaction conditions to obtain HCP-X-SO_3H in good to excellent yields (74–84% yield). The acid concentrations of these sulfonated polymers were determined to range from 3.81 to 4.11 mmol g^{-1}. The similar yields and acid concentrations of sterically different substrates suggested that the steric property of the substituent on the HCP-X had minimal effects on the efficiency of the sulfonation method.

2.2 Characterization of HCP-H-SO_3H

After synthesis, the HCP-X derivatives were characterized, using Fourier transform infrared (FTIR) spectroscopy. The FTIR spectra of HCP-H and HCP-H-SO_3H were shown in Fig. 1 and S3. The peaks located between 2900 and 3000 cm^{-1} corresponded to the C–H stretching vibration of methylene and benzene moieties. The peaks at approximately 1600 cm^{-1} corresponded

Table 1 Synthesis of hypercrosslinked porous organic polymer (HCP-X) and sulfonic-acid functionalized hypercrosslinked porous organic polymer (HCP-X-SO_3H)[a]

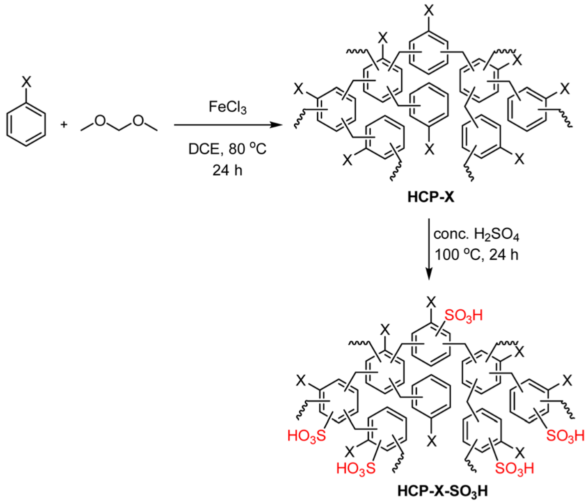

Entry	X =	Yield (%)		Acid concentration of HCP-X-SO_3H[c] (mmol g^{-1})
		HCP-X[a]	HCP-X-SO_3H[b]	
1	H	>99	78	4.16
2	CH_3	96	74	3.81
3	C_2H_5	>99	82	4.11
4	$^nC_3H_7$	99	84	3.95
5	$^iC_3H_7$	82	81	4.04

[a] Reaction conditions: benzene derivative (1.0 equiv.), dimethoxymethane (2.0 equiv.), and $FeCl_3$ (2.0 equiv.) in DCE (120 mL) at 80 °C for 24 h. [b] Reaction conditions: HCP-X (1.0 equiv.) and conc. H_2SO_4 (50.0 equiv.) at 100 °C for 24 h. [c] The acid concentration of HCP-X-SO_3H was calculated by the back acid-base titration method.

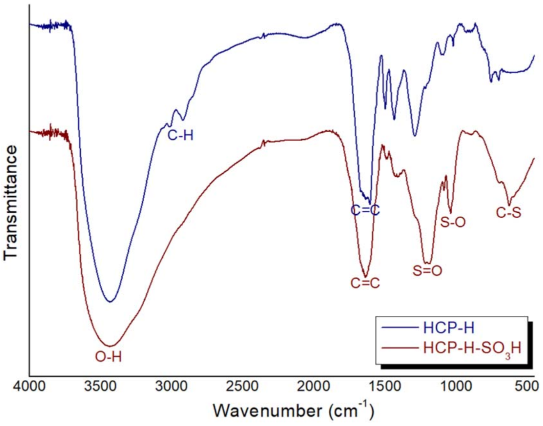

Fig. 1 FTIR spectra of HCP-H and HCP-H-SO$_3$H.

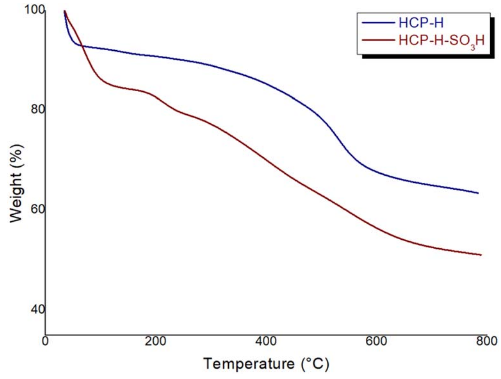

Fig. 3 TGA profiles of HCP-H and HCP-H-SO$_3$H.

to the C═C stretching vibrations of benzene in the skeletons of the HCPs. The new peaks corresponding to the sulfonic acid groups were found in the FTIR spectrum of HCP-H-SO$_3$H at approximately 1227 cm^{-1} and 1189 cm^{-1}, which corresponded to the symmetric and asymmetric O═S═O stretching of the sulfonic acid functional group.[21] The peaks at approximately 1037 cm^{-1} and 625 cm^{-1} were responsible for the S–O stretching vibration[21b,22] and the characteristic C–S stretching vibration,[19d,23] respectively. The FTIR data suggested a successful installation of the sulfonic acid functional group onto the surface of the porous hypercrosslinked organic polymer. Similar trends were also observed in other FTIR spectra of HCP-X and HCP-X-SO$_3$H (see SI).

To confirm the porous structure of HCP-H-SO$_3$H, the porosity and the surface area of the material were further investigated using N$_2$ adsorption–desorption analysis at 77 K (Fig. 2a). The HCP-H-SO$_3$H gave a typical type IV isotherm with a significant hysteresis loop, indicating the presence of micropores and mesopores in the network.[24] The adsorption isotherm displayed the steep nitrogen gas uptake at low relative pressure ($P/P_0 < 0.1$), which reflected the abundant microporous structure. The rise at higher pressure indicated the presence of the larger pores (mesopores and macropores) in the material. The N$_2$ sorption analysis exhibited a high Brunauer–Emmett–Teller (BET) surface area for HCP-H-SO$_3$H of about 604 m^2 g^{-1} with a total pore volume of approximately 0.41 cm^3 g^{-1}. The pore size distribution using the nonlocal density functional theory (NLDFT) for pillared clay model of the hypercrosslinked porous organic polymer after grafting of the sulfonic acid moiety exhibited a dominant pore width centered at ~0.88–1.45 nm (Fig. 2b), suggesting the microporous structure in the material. In addition, the mesopores were also found in the material. The presence of large pore in material is also good for performing acid catalyzed-intermolecular cyclization of small organic molecules.[25]

The thermal stabilities of the synthesized HCP-H and HCP-H-SO$_3$H were studied by thermogravimetric analysis (TGA) at a heating rate of 10 °C min^{-1} under nitrogen atmosphere in the temperature range of 35 to 800 °C (Fig. 3). The mass loss at the initial heating stage before 100 °C were about ~7% and ~14% in HCP-H and HCP-H-SO$_3$H, respectively owing to the evaporation of absorbed water molecules. The HCP-H was stable up to around 400 °C. A significant decrease in weight of about 25% was observed in the temperature range of 400 to 600 °C. On the other hand, the TGA plot of the HCP-H-SO$_3$H showed the thermal stability of HCP-H-SO$_3$H up to 200 °C before a sharp

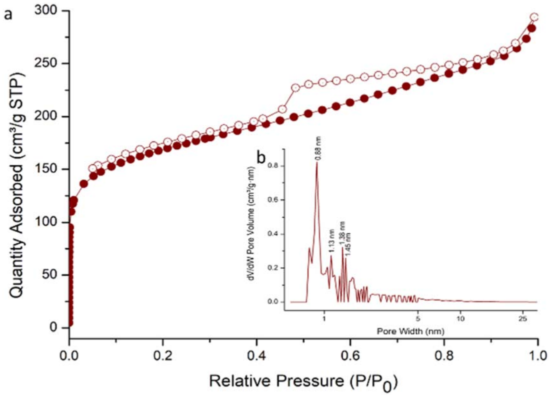

Fig. 2 (a) N$_2$ adsorption (closed symbols)–desorption (open symbols) isotherm and (b) pore size distribution calculated from NLDFT for pillared clay model of HCP-H-SO$_3$H

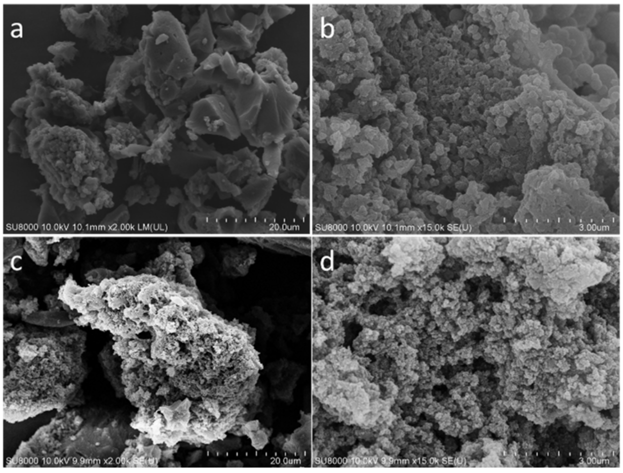

Fig. 4 FE-SEM images of (a) and (b) HCP-H and (c) and (d) HCP-H-SO$_3$H.

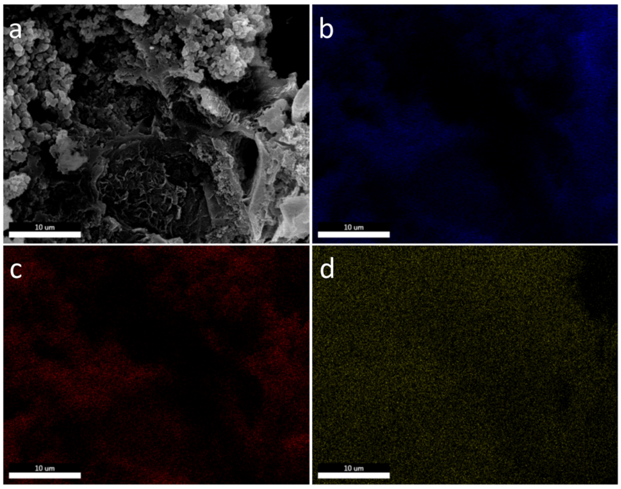

Fig. 5 (a) FE-SEM image and SEM-EDX elemental mappings of (b) carbon, (c) oxygen, and (d) sulfur for HCP-H-SO_3H.

decrease in weight of about 27% was observed in the temperature range of 250 to 650 °C.[26] The TGA results revealed that the materials were thermally stable at least up to 200 °C, which were in the compatibility range for the catalytic reaction of 2*H*-chromene synthesis.

The morphology of the HCP-H and HCP-H-SO_3H were studied using field-emission scanning electron microscopy (FE-SEM) images. As showed in Fig. 4, both materials retained the irregular and agglomerated small particles in a range of ten to hundred nanometers. The FE-SEM images also confirmed that the morphology of the polymers did not change during the sulfonation process (Fig. 4c and d). Moreover, scanning electron microscopy with energy-dispersive X-ray spectroscopy (SEM-EDX) elemental mapping showed that sulfur and oxygen elements were evenly distributed along with carbon elements on the surface of HCP-H-SO_3H (Fig. 5), revealing that sulfonic acid moiety were successfully introduced into the material. In addition, weight percentages of sulfur and oxygen increased to 8.13% and 32.65% in HCP-H-SO_3H compared to 0.37% and 23.83% in HCP-H, respectively (see SI).

2.3 Catalytic activity

The catalytic performance of the sulfonic-acid functionalized porous organic polymer HCP-H-SO_3H was investigated in the synthesis of 2*H*-chromene derivatives. The reaction between salicylaldehyde (**1a**) and dimethyl acethylenedicarboxylate (**2a**) was chosen as the model reaction to optimize the reaction conditions. To understand the effect of both the acidic polymeric catalyst and the basic organocatalyst on this reaction, several other catalysts were also examined (Table 2). In the absence of the amine organocatalyst, only unreacted starting material was recovered (entries 1–3). The reaction without the acidic polymeric catalyst and the reaction with non-sulfonated HCP-H gave only a trace amount of the product **3aa** (entries 4 and 5). The desired product **3aa** could be obtained in 20% yield, using a combination of HCP-H-SO_3H and pyrrolidine in

Table 2 Effect of catalysts on the reaction for the synthesis of 2*H*-chromene derivatives[a]

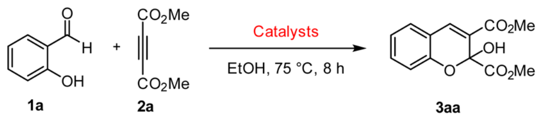

Entry	Catalyst (mol%)	Amine catalyst (mol%)	Yield[b] (%)
1	—	—	0
2	HCP-H (10 mg)	—	0
3	HCP-H-SO_3H (10)	—	0
4	—	Pyrrolidine (30)	Trace
5	HCP-H (10 mg)	Pyrrolidine (30)	Trace
6	HCP-H-SO_3H (2.5)	Pyrrolidine (30)	20
7	HCP-H-SO_3H (5)	Pyrrolidine (30)	24
8	**HCP-H-SO_3H (10)**	**Pyrrolidine (30)**	**62**
9	HCP-H-SO_3H (20)	Pyrrolidine (30)	51
10	HCP-H-SO_3H (10)	Piperidine (30)	38
11	HCP-H-SO_3H (10)	Piperazine (30)	41
12	HCP-H-SO_3H (10)	Benzylamine (30)	12
13	HCP-H-SO_3H (10)	DABCO (30)	0
14	HCP-H-SO_3H (10)	Pyrrolidine (10)	13
15	HCP-H-SO_3H (10)	Pyrrolidine (20)	32
16	HCP-H-SO_3H (10)	Pyrrolidine (40)	51
17	HCP-H-SO_3H (10)	Pyrrolidine (50)	51

[a] Reaction conditions: **1a** (0.25 mmol, 1 equiv.), **2a** (0.3 mmol, 1.2 equiv.), HCP-H-SO_3H (10 mol%), and pyrrolidine (30 mol%) in EtOH (0.5 mL) at 75 °C for 8 h. [b] Determined by crude ^1H NMR analysis.

Table 3 Optimization of the reaction conditions for HCP-H-SO_3H catalyzed 2*H*-chromenes synthesis[a]

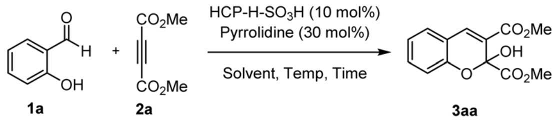

Entry	Solvent	Temp (°C)	Time	Yield[b] (%)
1	EtOH	75	8	62
2	MeOH	75	8	36
3	^{t}BuOH	75	8	49
4	^{i}PrOH	75	8	44
5	H_2O	75	8	16
6	THF	75	8	Trace
7	MeCN	75	8	Trace
8	EtOAc	75	8	Trace
9	PhMe	75	8	Trace
10	CH_2Cl_2	75	8	0
11	EtOH	RT	8	22
12	EtOH	60	8	26
13	EtOH	75	16	67
14	EtOH	75	24	59
15[c]	EtOH	75	16	75 (73)
16[d]	**EtOH**	**75**	**16**	**84 (79)**

[a] Reaction conditions: **1a** (0.25 mmol, 1 equiv.), **2a** (0.3 mmol, 1.2 equiv.), HCP-H-SO_3H (10 mol%), and pyrrolidine (30 mol%) in solvent (0.5 mL). [b] Determined by crude ^1H NMR analysis. The value in parenthesis is an isolated yield. [c] **2a** (0.375 mmol, 1.5 equiv.) was used for 16 h. [d] 1.0 mmol of **1a** scale.

Table 4 Substrate scope[a]

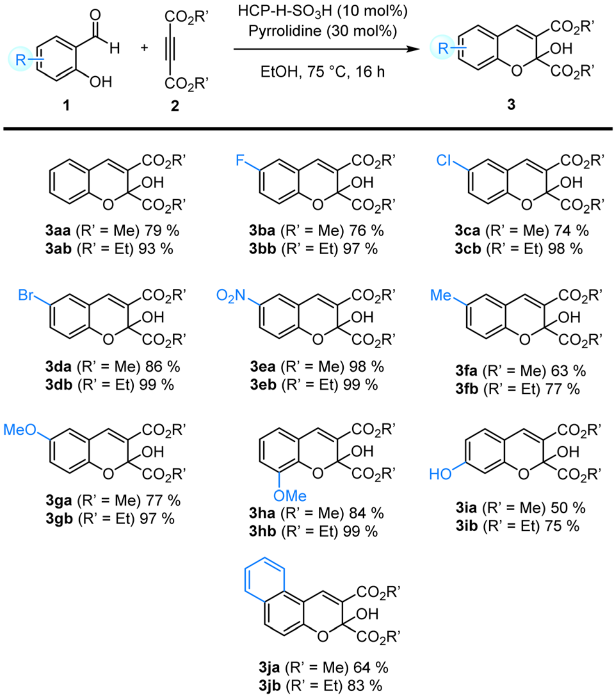

3aa (R' = Me) 79 %
3ab (R' = Et) 93 %

3ba (R' = Me) 76 %
3bb (R' = Et) 97 %

3ca (R' = Me) 74 %
3cb (R' = Et) 98 %

3da (R' = Me) 86 %
3db (R' = Et) 99 %

3ea (R' = Me) 98 %
3eb (R' = Et) 99 %

3fa (R' = Me) 63 %
3fb (R' = Et) 77 %

3ga (R' = Me) 77 %
3gb (R' = Et) 97 %

3ha (R' = Me) 84 %
3hb (R' = Et) 99 %

3ia (R' = Me) 50 %
3ib (R' = Et) 75 %

3ja (R' = Me) 64 %
3jb (R' = Et) 83 %

[a] Reaction conditions: salicylaldehyde **1a–j** (1.0 mmol, 1.0 equiv.), dialkyl acetylenedicarboxylate **2a–b** (1.5 mmol, 1.5 equiv.), HCP-H-SO_3H (10 mol%), and pyrrolidine (30 mol%) in EtOH (2.0 mL) at 75 °C for 16 h.

a catalytic amount (entry 6). This result suggested that both acidic and basic catalysts were crucial in this reaction. The catalytic loading of the HCP-H-SO_3H had a significant effect in the reaction. Increasing the acidic polymeric catalyst loading up to 10 mol% of HCP-H-SO_3H led to a higher yield of the product (entries 6–9). However, a higher amount of the catalyst (20 mol%) led to a decrease in the yield (entry 9). Next, the type of base was investigated. Other amines such as piperidine, piperazine, and benzylamine gave the desired product **3aa** in lower yields (entries 10–12). DABCO did not give any product (entry 13). Pyrrolidine was the optimal basic catalyst in the reaction, giving the product in the highest yield. Decreasing or increasing the pyrrolidine loading resulted in a reduction of the product yields (entries 14–17).

To further improve the yield of 2*H*-chromene **3aa**, other parameters were investigated (Table 3). The solvent screening was performed. Alcoholic solvents such as EtOH, MeOH, ^{t}BuOH, and ^{i}PrOH afforded the desired product **3aa** in 36–62% yields (entries 1–4). Water and aprotic solvents such as THF, MeCN, EtOAc, toluene, and CH_2Cl_2 were ineffective and gave **3aa** in lower yields (entries 5–10). Subsequently, the effect of reaction temperature and time was investigated. Decreasing the temperature from 75 °C to room temperature and 60 °C did not increase the yield of the product (entries 11 and 12). Increasing the reaction time from 8 to 16 hours gave **3aa** in 67% yield (entry 13); however, further prolonging the reaction time showed no improvement in the product yield (entry 14). Increasing the equivalent of **2a** to 1.5 equivalent improved the yield of **3aa** to 73% isolated yield (entry 15). The reaction also worked well at a larger scale, giving the product in 79% isolated yield (entry 16).

With the optimized reaction conditions in hand, we studied the substrate scope of the cyclization reaction using *ortho*-hydroxy aromatic aldehydes and dialkyl acethylene-dicarboxylates with various substituents (Table 4). Salicylaldehydes with different substituents worked well in the reaction, giving the 2*H*-chromene products in moderate to excellent yields. Substrates with electron-withdrawing substituents such as fluoro, chloro, bromo, and nitro groups provided the corresponding product **3ba–3ea** in 74–98% yields. In contrast, salicylaldehydes with electron donating substituents such as methoxy and methyl groups gave the desired products **3fa–3ha** in slightly lower yields (63–84%). The reaction of 2,5-dihydroxybenzaldehyde gave the desired product **3ia** in only 50% yield. In addition, the reaction of 2-hydroxy-1-naphthaldehyde gave the corresponding product **3ja** in 64% yield. When diethyl acethylenedicarboxylate **2b** was used instead of dimethyl acethylenedicarboxylate **2a**, the corresponding 2*H* chromene products **3ab–3jb** were obtained in good to excellent yields (75–99% yields).

2.4 Reusability of the catalyst

The recyclability of the heterogeneous hypercrosslinked porous organic polymer was investigated using the reaction of *o*-vanillin (**1h**) and alkynoic diester **2b** under the optimized reaction conditions as the model reaction (Table 5). After the completion of each run of the reaction, the HCP-H-SO_3H

Table 5 Recyclability of HCP-H-SO_3H catalyst in the synthesis of the 2*H*-chromene **3hb**[a]

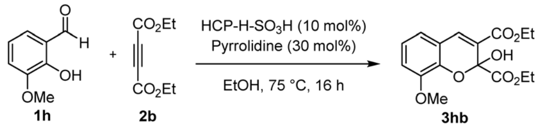

Run	Yield of **3hb** (%)
1	99
2	99
3	99
4	98
5	96

[a] Reaction conditions: **1h** (1.0 mmol, 1.0 equiv.) and **2b** (1.5 mmol, 1.5 equiv,), HCP-H-SO_3H (10 mol%), and pyrrolidine (30 mol%) in EtOH (2.0 mL) at 75 °C for 16 h.

catalyst was recovered by a simple filtration, washing, and drying processes. The catalyst can be used under the optimized reaction conditions for at least five consecutive runs with a minimal loss in the yields of the product. This result showed that the HCP-H-SO_3H catalyst was highly stable in the optimized reaction conditions.

2.5 Mechanistic investigation

Kinetic isotope effects (KIEs) is an important tool to study the change in bonding in the rate-determining step.[27] To gain further insight into the nature of the rate-limiting step in the catalytic cyclization of salicylaldehyde and dialkyl acetylenedicarboxylate, competitive ^{13}C KIEs were determined by natural abundant $^{12}C/^{13}C$ ratios using Singleton's ^{13}C NMR methodology for product analysis.[28] The reaction of 5-bromosalicylaldehyde (**1d**) and alkynoic diester **2a** catalyzed by an acid catalyst was chosen for the determination of experimental ^{13}C KIEs at natural abundance. The KIE measurements in the reaction were determined at low conversion to ensure that the faster reacting isotope of the product is enriched. Quantitative ^{13}C measurements were carried out for the reactions in the presence of HCP-H-SO_3H and PTSA·H_2O as the heterogeneous catalyst and the corresponding homogeneous catalyst, respectively. To determine the relative proportion of ^{13}C isotope compared to the original starting substrate, C_4 in **1d** and the methyl group (C_d) in **2a** were used as an internal standard with the assumption that its isotopic composition does not change (see SI).

Table 6 Natural abundance ^{13}C NMR kinetic isotope effects[a]

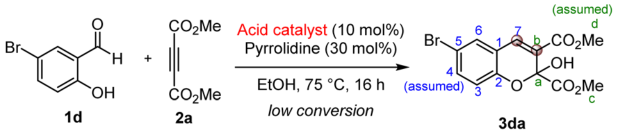

Quantitative ^{13}C KIEs		Acid catalyst PTSA·H_2O[b]	HCP-H-SO_3H[c]
KIEs determined from **1d**	C_1	1.001 (5)	1.000 (1)
	C_2	1.000 (2)	1.000 (1)
	C_4	1.000 (assumed)	
	C_5	1.003 (1)	0.999 (1)
	C_6	1.003 (1)	1.003 (2)
	$\mathbf{C_7}$	**1.039 (2)**	**1.043 (1)**
KIEs determined from **2a**	C_a	0.998 (2)	1.000 (1)
	$\mathbf{C_b}$	**1.022 (1)**	**1.023 (1)**
	C_c	1.001 (4)	1.000 (1)
	C_d	1.000 (assumed)	

[a] Experimental ^{13}C KIEs for product **3da**. [b] Three experiments were carried to 15%, 16%, and 17% conversion to determine the KIEs for PTSA·H_2O catalysis. [c] Three experiments were carried to 6%, 8%, and 10% conversion to determine the KIEs for HCP-H-SO_3H catalysis. Each reaction was performed in five independent quantitative ^{13}C NMR measurements. The numbers in parenthesis represent the standard deviation in the last digit.

The KIEs results were summarized in Table 6. The result from the reactions with PTSA·H_2O and HCP-H-SO_3H showed the same trend. The normal KIE was observed at C_7 and C_b of the product **3da**, indicating that both carbons were involved in the rate-determining step (RDS) in the catalytic process. Other carbon positions have near-unity KIEs. The results quantitatively validated our hypothesis that the carbon–carbon bond formation step may be important in the rate-determining step of the reaction and a plausible mechanism of 2*H*-chromene synthesis in the presence of HCP-H-SO_3H as an acid catalyst is similar to that of the homogeneous catalytic reaction.

From the basis of the results and previous reports,[4,29] a plausible mechanism for the formation of 2*H*-chromene products **3** in the presence of HCP-H-SO_3H and pyrrolidine as the catalysts was outlined in Scheme 1. First, the carbonyl group of *ortho*-hydroxy aromatic aldehydes was activated by HCP-H-SO_3H to form intermediate **I**. Meanwhile a conjugate addition reaction between acetylenic diester **2** and pyrrolidine gave the enamino ester intermediate **II**. Subsequently, the intermediate **II** reacted with the activated intermediate **I** to produce intermediate **III**. This step was proposed to be the rate-determining step. Next, an intramolecular nucleophilic attack by a hydroxyl group to the electron-deficient carbon atom of the iminium resulted in the six-membered ring intermediate **IV**. Subsequent elimination of pyrrolidine led to 4*H*-chromene intermediate **V**. Finally, transformation of the intermediate **V** to the desired 2*H*-chromene product **3** occurred *via* an isomerization process through a benzopyrylium intermediate **VI**.

3 Experimental section

3.1 General information

All reactions were performed under an ambient atmosphere in oven-dried glassware with magnetic stirrer. Reactions conducted above an ambient temperature were heated by an anodized aluminum block. Starting reagents and organic solvents were purchased from commercial sources (Sigma-Aldrich, TCI, Merck, and Alfa Aesar) and were used without further purification unless otherwise noted. Analytical thin layer chromatography (TLC) was performed on alumina sheets pre-coated with a Merck silica gel 60 F254 plate and compounds

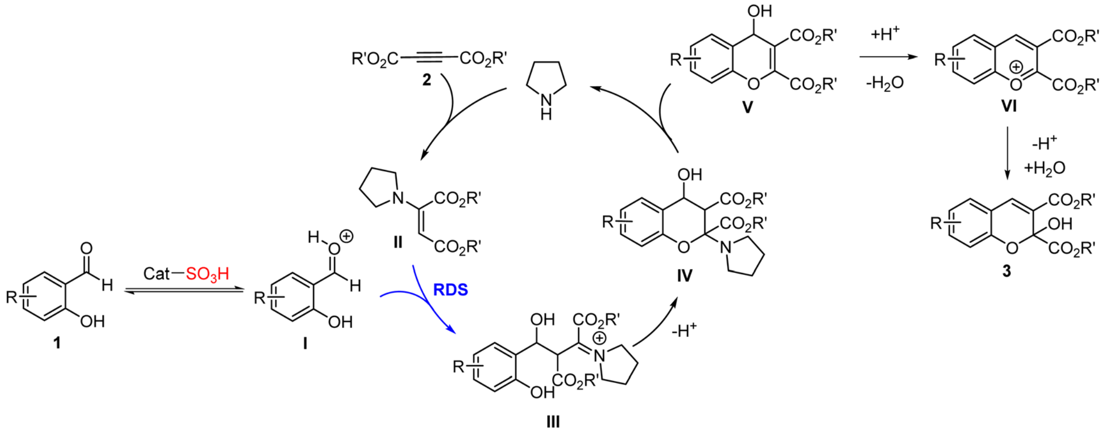

Scheme 1 Plausible reaction mechanism for the intermolecular cyclization reaction of *ortho*-hydroxy aromatic aldehydes with acetylenic diesters catalyzed by solid-acid HCP-H-SO_3H in the presence of pyrrolidine.

were visualized under UV light. Purification of reaction products was carried out by column chromatography, in which a Merck silica gel 60 (0.063–0.200 mm) was used as a stationary phase. Proton nuclear magnetic resonance (^{1}H NMR) and proton-decoupled carbon nuclear magnetic resonance (^{13}C NMR) spectra were recorded on a Bruker Avance 400 MHz and JEOL 400 MHz NMR spectrometer in deuterated chloroform ($CDCl_3$) and deuterated acetone ($(CD_3)_2CO$). The chemical shifts were recorded in part per million (ppm) relative to the resonance of the residual protonated solvent (^{1}H: $CDCl_3$, δ = 7.24 ppm; acetone-d$_6$, δ = 2.05 ppm and ^{13}C: $CDCl_3$, δ = 77.23 ppm; acetone-d$_6$, δ = 29.84 ppm). Data are reported as following: (brs = broad, s = singlet, d = doublet, t = triplet, m = multiplet, dd = doublet of doublet, td = triplet of doublet; coupling constants, *J*, in Hz, integration). Melting points were determined in open glass capillaries using a Buchi melting point M-565 apparatus. FTIR spectra were recorded on a PerkinElmer Frontier FTIR spectrometer. The nitrogen adsorption–desorption isotherm (77 K) was obtained using Micromeritics 3Flex gas sorption analyser. Surface area was calculated in the range of 0.05–0.15 P/P_0 using Brunauer–Emmett–Teller (BET) theory. TGA was performed under a flow of nitrogen by heating from room temperature to 800 °C with 10 °C min^{-1} on TA Instruments SDT 2960. SEM and EDX data were obtained from Field Emission Scanning Electron Microscopes (FE-SEM) (HITACHI SU-8010) mass spectrometric data were obtained with high resolution mass spectra (HRMS) on a Bruker micrOTOF spectrometer in the ESI mode.

3.2 Synthesis of HCP-H

To a solution of benzene (4.68 g, 60 mmol, 1.0 equiv.) and dimethoxymethane (9.13 g, 120 mmol, 2.0 equiv.) in dichloroethane 120 mL was added $FeCl_3$ (19.5 g, 120 mmol, 2.0 equiv.). The reaction was refluxed with stirring for 24 hours. The reaction was filtered. The brown solid was washed with methanol by a Soxhlet extractor until the yellow solution changed to colorless. The brown solid was dried in an oven for 24 hours. The reaction gave a brown solid as the product (3.60 g, quantitative yield).

3.3 Synthesis of HCP-H-SO_3H and acid concentration measurement

The reaction of HCP-H (2.01 g, 20 mmol, 1.0 equiv.) in conc. H_2SO_4 (56 mL, 50 equiv.) was stirred at 100 °C for 24 hours. The reaction was washed with H_2O until the pH of the aqueous solution was neutral. The black solid was dried in an oven for 24 hours. The reaction gave a black solid as the product (2.80 g, 78%). The acid concentration was calculated by a back titration method. HCP-H-SO_3H (20 mg, 0.2 mmol, 1.0 equiv.) was stirred with 0.0250 M NaOH (10 mL) for 1 hour. After that, the reaction was filtered and washed with water until the pH was neutral. The volume of the aqueous phase was adjusted to 100 mL, and 10 mL of the solution was pipetted to a flask containing 0.0250 M HCl solution (10 mL). The solution was titrated with 0.0125 M NaOH. The acid concentration in HCP-H-SO_3H was determined to be 4.16 mmol g^{-1}.

3.4 General procedure for the synthesis of 2*H*-chromene derivatives

To a suspension of salicylaldehydes (**1a–j**, 1.0 mmol, 1.0 equiv.) and HCP-H-SO_3H (0.10 mmol, 10 mol%) in ethanol (2.0 mL) was added dialkyl acetylenedicarboxylate (**2a–b**, 1.5 mmol, 1.5 equiv.) and pyrrolidine (24.6 µL, 0.30 mmol, 30 mol%). The reaction was stirred at 75 °C for 16 hours. The reaction mixture was filtered through a PTFE syringe filter, and the filter was thoroughly washed successively with water, methanol, and acetone. The filtrate was extracted with EtOAc, washed with brine, dried over anhydrous Na_2SO_4, and filtered. The solvent was removed *in vacuo*, and the crude product was purified by flash column chromatography (silica gel: EtOAc/hexane) to give the pure product **3**.

3.5 Recycling of the HCP-H-SO_3H catalyst

After completion of the catalytic reaction, the acid catalyst HCP-H-SO_3H was recovered through filtration for further use and thoroughly washed successively with water, methanol, and acetone. Then the recovered catalyst was dried overnight in an oven 120 °C.

3.6 ^{13}C NMR kinetic isotope effects at natural abundance

The reaction between 5-bromosalicylaldehyde (**1d**) and dimethylacethylenedicarboxylate (**2a**) were chosen to determine the KIEs. The PTSA·H_2O catalyzed cyclization reaction was repeated three times, giving the following yields: 15%, 16%, and 17%. The HCP-H-SO_3H catalyzed cyclisation reaction was repeated three times, giving the following yields: 6%, 8%, and 10%. The percent yield of product was assumed as percent conversion. Two reference starting materials (**1d** and **2a**) were used. The NMR samples were prepared in deuterated chloroform ($CDCl_3$). The quantitative ^{13}C NMR spectra were taken at 100 MHz on a Bruker Avance 400 MHz NMR spectrometer with inverse-gated ^{1}H decoupling which used 30° pulses (zgig30 pulse program). Acquisition parameters were as follows: acquisition time 5.2 s; spectral width 240 ppm, size of fid 250k; recovery delays 75 s; size of real spectrum 64k points; transmitter frequency offset 110 ppm; number of dummy scans 8; pre-scan delay 50 μs; number of scans 512. ^{13}C NMR measurements were carried out for the KIE values of the product **3da**. ^{13}C NMR data were processed using 1 Hz exponential multiplication. For the KIE determination, the integration of C_4 was set to 100 when **1d** was used as a reference, and the integration of C_d was set to 100 when **2a** as a reference. The average integration values for the other carbons were used to calculate the KIE values using eqn (1).

$$\mathrm{KIE}_{\mathrm{calc}} = \frac{\ln(1-F)}{\ln\left[1-\left(F\frac{R_{\mathrm{P}}}{R_0}\right)\right]} \quad (1)$$

where F is the fraction of reaction and R_{P} and R_0 are the isotope ratio of residual product, and initial starting substrate at fraction of reaction, respectively.

4 Conclusions

In summary, sulfonic-acid functionalized hypercrosslinked porous organic polymers (HCP-X-SO_3H) were successfully prepared by a Friedel–Crafts alkylation and a sulfonation using readily available sulfuric acid. HCP-H-SO_3H was used as an efficient heterogeneous catalyst for the synthesis of 2*H*-chromene derivatives from various *ortho*-hydroxy aromatic aldehydes and acetylenic diesters under mild reaction conditions. The catalyst could be recovered and reused for at least five times with minimal loss in the product yield. Mechanistic investigation of the cyclization reaction with heterogeneous HCP-H-SO_3H catalyst and that with homogeneous PTSA·H_2O catalyst using ^{13}C KIEs suggested that the nature of their rate-determining steps was similar. Due to their high catalytic efficiency and stability, the sulfonic-acid functionalized hypercrosslinked porous organic polymers have great potential as an efficient heterogeneous acid catalyst for a wide range of mechanistically complex reactions. Application of the catalyst for other reactions is ongoing and will be reported in due course.

Author contributions

Siriphong Somprasong designed the project, optimized the reaction conditions, investigated the substrate scope, analyzed the data, performed the mechanistic experiments, and wrote the draft of the manuscript. Thanchanok Ratvijitvech designed the project, synthesized and characterized hypercrosslinked porous organic polymers, analyzed the data, wrote the draft of the manuscript, and edited the manuscript. Thanakorn Tiyawarakul synthesized and characterized hypercrosslinked porous organic polymers. Chaiwat Rujirasereesakul performed mechanistic experiments. Thanakorn Sitthasakul performed mechanistic experiments. Torsak Luanphaisarnnont designed the project, analyzed the data, supervised the project, secured the funding, wrote the draft of the manuscript, and edited the manuscript. All the authors contributed to and approved the final version of the manuscript.

Conflicts of interest

There are no conflicts to declare.

Data availability

Experimental and analytical data supporting this article are available in the supplementary information (SI). Supplementary information is available. See DOI: https://doi.org/10.1039/d6ra03062a.

Acknowledgements

This research was supported by Mahidol University (Fundamental Fund: fiscal year 2025 by National Science Research and Innovation Fund (NSRF), FF-075/2568). Support from the Center of Excellence for Innovation in Chemistry (PERCH-CIC), Ministry of Higher Education, Science, Research and Innovation is gratefully acknowledged. We are also grateful for the support from the Department of Chemistry and the Central Instrumental Facility (CIF), Faculty of Science, Mahidol University for research facilities.

Notes and references

1 (*a*) N. Majumdar, N. D. Paul, S. Mandal, B. de Bruin and W. D. Wulff, *ACS Catal.*, 2015, **5**, 2329–2366; (*b*) R. Pratap and V. J. Ram, *Chem. Rev.*, 2014, **114**, 10476–10526.

2 (*a*) A. D. Pugachev, M. B. Lukyanova, B. S. Lukyanov, I. V. Ozhogin, A. S. Kozlenko, I. A. Rostovtseva, N. I. Makarova, V. V. Tkachev and N. A. Aksenov, *J. Mol. Struct.*, 2019, **1178**, 590–598; (*b*) Y. Yue, C. Yin, F. Huo, J. Chao and Y. Zhang, *Sens. Actuators, B*, 2016, **223**, 496–500; (*c*) S. N. Corns, S. M. Partington and A. D. Towns, *Color. Technol.*, 2009, **125**, 249–261.

3 For selected examples of synthesis of 2*H*-chromenes, see: (*a*) Q. J. Yang, Y. B. Wang, S. H. Luo and J. Wang, *Angew. Chem., Int. Ed.*, 2019, **58**, 5343–5347; (*b*) P. N. Moquist, T. Kodama and S. E. Schaus, *Angew. Chem., Int. Ed.*, 2010, **49**, 7096–7100; *Angew. Chem.*, 2010, **122**, 7250–7254; (*c*) H. Hu, K.-Y. Ye, Q.-F. Wu, L.-X. Dai and S.-L. You, *Adv. Synth. Catal.*, 2012, **354**, 1084–1094; (*d*) B.-S. Zeng, X.-Y. Yu, P. W. Siu and K. A. Scheidt, *Chem. Sci.*, 2014, **5**, 2277–2281;

(*e*) H. Li, J. Wang, T. E-Nunu, L. Zu, W. Jiang, S. Wei and W. Wang, *Chem. Commun.*, 2007, **43**, 507–509; (*f*) D.-Q. Xu, Y.-F. Wang, S.-P. Luo, S. Zhang, A.-G. Zhong, H. Chen and Z.-Y. Xu, *Adv. Synth. Catal.*, 2008, **350**, 2610–2616; (*g*) H. Cai, L. Xia, Y. R. Lee, J.-J. Shim and S. H. Kim, *Eur. J. Org Chem.*, 2015, 5212–5220; (*h*) G. Maiti, R. Karmakar, U. Kayal and R. N. Bhattacharya, *Tetrahedron*, 2012, **68**, 8817–8822; (*i*) J. Yang, J.-N. Tan and Y. Gu, *Green Chem.*, 2012, **14**, 3304–3317; (*j*) M. Rueping, U. Uria, M.-Y. Lin and I. Atodiresei, *J. Am. Chem. Soc.*, 2011, **133**, 3732–3735.

4 S. Somprasong, W. Prasitwatcharakorn and T. Luanphaisarnnont, *Tetrahedron Lett.*, 2020, **61**, 152402.

5 (*a*) J. M. Thomas, R. Raja and D. W. Lewis, *Angew. Chem., Int. Ed.*, 2005, **44**, 6456–6482; (*b*) A. Álvarez, A. Bansode, A. Urakawa, A. V. Bavykina, T. A. Wezendonk, M. Makkee, J. Gascon and F. Kapteijn, *Chem. Rev.*, 2017, **117**, 9804–9838; (*c*) L. Liu and A. Corma, *Chem. Rev.*, 2018, **118**, 4981–5079; (*d*) K. Huang, J.-Y. Zhang, F. Liu and S. Dai, *ACS Catal.*, 2018, **8**, 9079–9102; (*e*) S. Kim, E. E. Kwon, Y. T. Kim, S. Jung, H. J. Kim, G. W. Hubere and J. Lee, *Green Chem.*, 2019, **21**, 3715–3743; (*f*) H. Liu, L. Wei, F. Liu, Z. Pei, J. Shi, Z.-J. Wang, D. He and Y. Chen, *ACS Catal.*, 2019, **9**, 5245–5267; (*g*) S. De, A. Dokania, A. Ramirez and J. Gascon, *ACS Catal.*, 2020, **10**, 14147–14185; (*h*) R. Nie, Y. Tao, Y. Nie, T. Lu, J. Wang, Y. Zhang, X. Lu and C. Xu, *ACS Catal.*, 2021, **11**, 1071–1095.

6 (*a*) Z. Chang, D.-S. Zhang, Q. Chen and X.-H. Bu, *Phys. Chem. Chem. Phys.*, 2013, **15**, 5430–5442; (*b*) H. Furukawa and O. M. Yaghi, *J. Am. Chem. Soc.*, 2009, **131**, 8875–8883; (*c*) T. Ben, C. Pei, D. Zhang, J. Xu, F. Deng, X. Jing and S. Qiu, *Energy Environ. Sci.*, 2011, **4**, 3991–3999; (*d*) R. Dawson, A. I. Cooper and D. J. Adams, *Polym. Int.*, 2013, **62**, 345–352; (*e*) P. Lindemann, M. Tsotsalas, S. Shishatskiy, V. Abetz, P. KrollaSidenstein, C. Azucena, L. Monnereau, A. Beyer, A. Gölzhäuser, V. Mugnaini, H. Gliemann, S. Bräse and C. Wöll, *Chem. Mater.*, 2014, **26**, 7189–7193; (*f*) R. T. Woodward, L. A. Stevens, R. Dawson, M. Vijayaraghavan, T. Hasell, I. P. Silverwood, A. V. Ewing, T. Ratvijitvech, J. D. Exley, S. Y. Chong, F. Blanc, D. J. Adams, S. G. Kazarian, C. E. Snape, T. C. Drage and A. I. Cooper, *J. Am. Chem. Soc.*, 2014, **136**(25), 9028–9035.

7 (*a*) K. V. Rao, S. Mohapatra, T. K. Maji and S. J. George, *Chem.–Eur. J.*, 2012, **18**, 4505–4509; (*b*) J. F. Van Humbeck, T. M. McDonald, X. Jing, B. M. Wiers, G. Zhu and J. R. Long, *J. Am. Chem. Soc.*, 2014, 2432–2440; (*c*) B. Li, F. Su, H.-K. Luo, L. Liang and B. Tan, *Microporous Mesoporous Mater.*, 2011, **138**, 207–214; (*d*) T. Ratvijitvech, *J. Polym. Environ.*, 2020, **28**, 2211–2218.

8 S. Bhunia, N. Chatterjee, S. Das, K. Das Saha and A. Bhaumik, *ACS Appl. Mater. Interfaces*, 2014, **6**, 22569–22576.

9 (*a*) T. Ratvijitvecha and S. Na Pombejra, *Mater. Today Commun.*, 2021, **28**, 102617; (*b*) D. Li, Y. Fang and X. Zhang, *ACS Appl. Mater. Interfaces*, 2020, **12**(8), 8989–8999; (*c*) A. Mohan, M. H. Al-Sayah, A. Ahmed and O. M. El-Kadri, *Sci. Rep.*, 2022, **12**, 2638.

10 (*a*) Y. Xu, L. Chen, Z. Guo, A. Nagai and D. Jiang, *J. Am. Chem. Soc.*, 2011, **133**, 17622–17625; (*b*) J. X. Jiang, A. Trewin, D. J. Adams and A. I. Cooper, *Chem. Sci.*, 2011, **2**, 1777–1781; (*c*) L. Chen, Y. Honsho, S. Seki and D. Jiang, *J. Am. Chem. Soc.*, 2010, **132**, 6742–6748.

11 X. Liu, Y. Xu and D. Jiang, *J. Am. Chem. Soc.*, 2012, **134**, 8738–8741.

12 (*a*) F. Vilela, K. Zhang and M. Antonietti, *Energy Environ. Sci.*, 2012, **5**, 7819–7832; (*b*) R. S. Sprick, J.-X. Jiang, B. Bonillo, S. Ren, T. Ratvijitvech, P. Guiglion, M. A. Zwijnenburg, D. J. Adams and A. I. Cooper, *J. Am. Chem. Soc.*, 2015, **137**, 3265–3270; (*c*) Y. Kou, Y. Xu, Z. Guo and D. Jiang, *Angew. Chem., Int. Ed.*, 2011, **50**, 8753–8757.

13 (*a*) P. Kaur, J. T. Hupp and S. T. Nguyen, *ACS Catal.*, 2011, **1**, 819–835; (*b*) Y. Zhang and S. N. Riduan, *Chem. Soc. Rev.*, 2012, **41**, 2083–2094; (*c*) C. Thiamsiri, T. Ratvijitvech and T. Luanphaisarnnont, *Mater. Adv.*, 2023, **4**, 5184–5190; (*d*) P. Schweng, D. Guerin-Faucheur, F. Kleitz and R. T. Woodward, *Chem. Commun.*, 2024, **60**, 14395–14398.

14 N. Noshiranzadeh and A. Ramazani, *Synth. Commun.*, 2007, **37**, 3181–3189.

15 H. Valizadeh, L. Dinparast, S. Noorshargh and M. M. Heravi, *C. R. Chem.*, 2016, **19**, 395–402.

16 L. Dinparast and H. Valizadeh, *Monatsh. Chem.*, 2015, **146**, 313–319.

17 (*a*) R. M. N. Kalla, M.-R. Kim and I. Kim, *Ind. Eng. Chem. Res.*, 2018, **57**, 11583–11591; (*b*) S. S. Reddy, R. M. N. Kalla, A. Varyambath and I. Kim, *Catal. Commun.*, 2019, **126**, 15–20; (*c*) A. Blocher, F. Mayer, P. Schweng, T. M. Tikovits, N. Yousefi and R. T. Woodward, *Mater. Adv.*, 2022, **3**, 6335–6342.

18 (*a*) W. Guan, C.-W. Tsang, C. S. K. Lin, C. Len, H. Hu and C. Lianga, *Bioresour. Technol.*, 2020, **298**, 122432; (*b*) S. M. Silva, A. F. Peixoto and C. Freire, *Renewable Energy*, 2020, **146**, 2416–2429; (*c*) S. M. Silva, A. F. Peixoto and C. Freire, *Appl. Catal., A*, 2020, **568**, 221–230; (*d*) S. Mondal, J. Mondal and A. Bhaumik, *ChemCatChem*, 2015, **7**, 3570–3578; (*e*) M. Du, A. M. Agrawal, S. Chakraborty, S. J. Garibay, R. Limvorapitux, B. Choi, S. T. Madrahimov and S. T. Nguyen, *ACS Sustainable Chem. Eng.*, 2019, **7**, 8126–8135; (*f*) B. Agarwal, K. Kailasam, R. S. Sangwan and S. Elumalai, *Renewable Sustainable Energy Rev.*, 2018, **82**, 2408–2425; (*g*) R. T. Woodward, M. Kessler, S. Lima and R. Rinaldi, *Green Chem.*, 2018, **20**, 2374–2381.

19 (*a*) J. R. Pereira, M. C. Corvo, A. F. Peixoto, A. Aguiar-Ricardo and M. M. B. Marques, *ChemCatChem*, 2023, **15**, e202201318; (*b*) A. Y. Sidorenko, N. S. Li-Zhulanov, P. Mäki-Arvela, T. Sandberg, A. V. Kravtsova, A. F. Peixoto, C. Freire, K. P. Volcho, N. F. Salakhutdinov, V. E. Agabekov and D. Yu Murzin, *ChemCatChem*, 2020, **12**, 2605–2609; (*c*) L. Sekerová, P. Březinová, T. T. Do, E. Vyskočilová, J. Krupka, L. Červený, L. Havelková, B. Bashta and J. Sedláček, *ChemCatChem*, 2020, **12**, 1075–1084; (*d*) S. Mondal, B. C. Patra and A. Bhaumik, *ChemCatChem*, 2017, **9**, 1469–1475; (*e*) B. Li, K. Leng, Y. Zhang, J. J. Dynes, J. Wang, Y. Hu, D. Ma, Z. Shi, L. Zhu, D. Zhang, Y. Sun, M. Chrzanowski and S. Ma, *J. Am. Chem. Soc.*, 2015, **137**,

4243–4248; (*f*) M. Hara, T. Yoshida, A. Takagaki, T. Takata, J. N. Kondo, S. Hayashi and K. Domen, *Angew. Chem., Int. Ed.*, 2004, **43**, 2955–2958.

20 R. Dawson, T. Ratvijitvech, M. Corker, A. Laybourn, Y. Z. Khimyak, A. I. Cooper and D. J. Adams, *Polym. Chem.*, 2012, **3**, 2034–2038.

21 (*a*) J. Juan-Alcañiz, R. Gielisse, A. B. Lago, E. V. Ramos-Fernandez, P. Serra-Crespo, T. Devic, N. Guillou, C. Serre, F. Kapteijna and J. Gasco, *Catal. Sci. Technol.*, 2013, **3**, 2311–2318; (*b*) M. G. Goesten, À. Szécsényi, M. F. de Lange, A. V. Bavykina, K. B. Sai Sankar Gupta, F. Kapteijn and J. Gascon, *ChemCatChem*, 2016, **8**, 961–967.

22 S. Suganuma, K. Nakajima, M. Kitano, S. Hayashi and M. Hara, *ChemSusChem*, 2012, **5**, 1841–1846.

23 W.-Y. Lou, Q. Guo, W.-J. Chen, M.-H. Zong, H. Wu and T. J. Smith, *ChemSusChem*, 2012, **5**, 1533–1541.

24 R. Gomes and A. Bhaumik, *J. Solid State Chem.*, 2015, **222**, 4–11.

25 B. Coasne, *New J. Chem.*, 2016, **40**, 4078–4094.

26 (*a*) M. Halder, P. Bhanja, M. M. Islam, S. Chatterjee, A. Khan, A. Bhaumik and S. ManirulIslam, *Mol. Catal.*, 2020, **494**, 111119; (*b*) K. Dong, J. Zhang, W. Luo, L. Su and Z. Huang, *Chem. Eng. Sci.*, 2018, **334**, 1055–1064.

27 For selected examples of isotope effects reveal the catalytic mechanism, see: (*a*) D. T. Nowlan III, T. M. Gregg, H. M. L. Davies and D. A. Singleton, *J. Am. Chem. Soc.*, 2003, **125**, 15902–15911; (*b*) L. K. Vo and D. A. Singleton, *Org. Lett.*, 2004, **6**, 2469–2472; (*c*) D. A. Singleton and Z. Wang, *J. Am. Chem. Soc.*, 2005, **127**, 6679–6685; (*d*) J. A. Izzo, P. H. Poulsen, J. A. Intrator, K. A. Jorgensen and M. J. Vetticatt, *J. Am. Chem. Soc.*, 2018, **140**, 8396–8400; (*e*) M. V. Joannou, J. M. Hoyt and P. J. Chirik, *J. Am. Chem. Soc.*, 2020, **142**, 5314–5330; (*f*) Y. Lin, W. J. Hirschi, A. Kunadia, A. Paul, I. Ghiviriga, K. A. Abboud, R. W. Karugu, M. J. Vetticatt, J. S. Hirschi and D. Seidel, *J. Am. Chem. Soc.*, 2020, **142**, 5627–5635; (*g*) J. N. Sanders, H. Jun, R. A. Yu, J. L. Gleason and K. N. Houk, *J. Am. Chem. Soc.*, 2020, **142**, 16877–16886; (*h*) K.-Y. Kuan and D. A. Singleton, *J. Org. Chem.*, 2021, **86**, 6305–6313; (*i*) V. Wambua, J. S. Hirschi and M. J. Vetticatt, *ACS Catal.*, 2021, **11**, 60–67; (*j*) C. Joshi, J. M. Macharia, J. A. Izzo, V. Wambua, S. Kim, J. S. Hirschi and M. J. Vetticatt, *ACS Catal.*, 2022, **12**, 2959–2966; (*k*) S. C. Mallojjala, V. O. Nyagilo, S. A. Corio, A. Adili, A. Dagar, K. A. Loyer, D. Seidel and J. S. Hirschi, *J. Am. Chem. Soc.*, 2022, **144**, 17692–17699; (*l*) S. Somprasong, M. Castiñeira Reis and S. R. Harutyunyan, *Angew. Chem., Int. Ed.*, 2023, **62**, e202217328; (*m*) S. Somprasong, M. Castiñeira Reis and S. R. Harutyunyan, *ACS Catal.*, 2024, **14**, 13030–13039; (*n*) S. Somprasong, B. Wan and S. R. Harutyunyan, *Chem. Sci.*, 2025, **16**, 802–808.

28 (*a*) D. E. Frantz, D. A. Singleton and J. P. Snyder, *J. Am. Chem. Soc.*, 1997, **119**, 3383–3384; (*b*) D. E. Frantz and D. A. Singleton, *J. Am. Chem. Soc.*, 2000, **122**, 3288–3295; (*c*) M. J. Vetticatt and D. A. Singleton, *Org. Lett.*, 2012, **14**, 2370–2373; (*d*) S. Xiang and M. P. Mayer, *J. Am. Chem. Soc.*, 2014, **136**, 5832–5835; (*e*) D. E. Frantz and D. A. Singleton, *J. Am. Chem. Soc.*, 2000, **122**, 3288–3295.

29 (*a*) P. Saejong, S. Somprasong, C. Rujirasereesakul and T. Luanphaisarnnont, *Synlett*, 2022, **33**, 1399–1404; (*b*) C. Kiattisewee, A. Kaidad, C. Jiarpinitnun and T. Luanphaisarnnont, *Monatsh. Chem.*, 2018, **149**, 1059.